materials

MDPI

Article

Influence of duty cycle of pulse electrodeposition coated Ni-Al_2O_3 nanocomposites over surface roughness properties

Aashish John [1], Adil Saeed [1] and Zulfiqar A Khan [1,*]

[1] NanoCorr, Energy & Modelling (NCEM) Research Group, Department of Design & Engineering, Bournemouth University, Talbot Campus, Dorset BH12 5BB, United Kingdom.

* Correspondence: zkhan@bournemouth.ac.uk

Abstract: This research presents the viability of duty cycle variation was explored as a potential method to improve mechanical and surface roughness properties of Ni-Al_2O_3 nanocoatings through pulse electrodeposition. Areal and surface roughness properties of nanocomposite pulse electrodeposition coated materials with varying duty cycle from 20% to 100% was studied, along with the analysis of bearing area curve and power spectral densities. Results demonstrate that with decrease in duty cycle, an enhancement in aerial roughness properties from 0.348 μm to 0.195 μm and surface roughness properties from 0.779 μm to 0.245 μm was observed. The change in surface roughness was due to grain size variation, resulting from the varying time intervals during pulse coatings. This increase in grain size during change in duty cycle was confirmed with the scanning electron microscope. In addition to that, increase in grain size from 0.32 μm to 0.92 μm with increase in duty cycle resulted in decrease in nanohardness from 4.21 GPa to 3.07 GPa. This work will provide a novel method for obtaining Ni-Al_2O_3 nanocomposite coating with improved surface roughness and hardness properties for wider industrial applications.

Keywords: keyword 1; Pulse electrodeposition coating 2; nanocomposites 3; surface roughness 4; Ni-Al_2O_3

1. Introduction

Within the last decade, pulse electrodeposition coatings have been considered as a simple, economic, and viable methodology for producing metal matrix composite (MMC) coating exhibiting high mechanical, tribological properties and corrosion-resistant properties [1–6]. Pulse electrodeposition is an augmentation of electrodeposition coating wherein various physical parameters including peak current density, duty cycle, frequency, pH and bath composition of electrolyte can be precisely controlled for obtaining remarkable surface coatings [7–10]. Hard particles dispersed with pulse electrodeposition methods for developing nanocomposite coatings and their resulting enhanced properties, have earned wide acceptance in chemical, mechanical and electronic industries [3,11–13]. The advantageous properties of pulse electrodeposition coating such as low cost, easy design, reduced grain size, high production rates and fever technological barriers results in the easy conversion from laboratory state to industrial scale [7,14,15].

Nickel-based nanocomposites exhibit outstanding properties and are therefore widely used in various petrochemical, mechanical, electromechanical and tribological applications. It has been widely known that by supplementing ceramic nanoparticles such as Al_2O_3, SiC, ZrO_2, MnO, ZrO, TiN, etc further improves coating surface characteristics. It has been reported that Ni-Al_2O_3 composite coating, developed through pulse electrodeposition techniques, hardness and tribological properties are affected by both frequency

Citation: To be added by editorial staff during production.

Academic Editor: Firstname Lastname

Received: date
Accepted: date
Published: date

and duty cycle [16]. It has been noticed that relatively low frequency and lower duty cycle result in enhanced tribological properties including hardness. It was added that pulse electrodeposition properties can have an influence on hardness and wear characteristics of coating without any alterations in the bath composition. Jegan et al. [17] employed Watt solution for Ni-Al_2O_3 nanocomposite coating by changing duty cycle, current density and frequency during deposition of coatings. It was espied that duty cycle was a predominant factor which influences hardness of the specimen. Chen et al. [18] varied frequency of pulse electrodeposition coating for Ni-Al_2O_3 and espied that increase in frequency resulted in decrease in hardness of composite coatings. Steinbach et al. [19] espied the lower agglomeration of particles during coating for pulsed electrodeposition coating than direct deposition coating. Along with this, smaller the particles used for coating more effective will it be to pin grain boundaries which will help in improving hardness of the surface. Ma et al. [20] fabricated Ni-Al_2O_3 coating with the help of ultrasonic-assisted electrodeposition method. It was observed that ultrasonic power affected the number of particles which had been incorporated on the surface in addition to their surface roughness. The increase in the ultrasonic power resulted in a change in hardness of the coated surface. The impact of current density on the pulse electrodeposition coating was studied by Gul et al. [21] with Al_2O_3 nanoparticles embedded with Ni. Increase of Al_2O_3 deposition has been observed with increasing current density, which resulted in increase of microhardness. During ON time, particles will be attached to surface due to the current provided and during OFF time, particles which are loosely adsorbed will be detached. During OFF state, loosely attached agglomerated particles will fall back to the electrolyte. With increase in current density, particles attached on to cathodic surface increases. It was concluded that microhardness enhancement has resulted from a decrease in the grain size and increasing current density. Along with it, it was noted that pulsed electrodeposition coating was having an improved properties compared to direct electrodeposition coating in all the current densities.

The properties of pulse electrodeposited coatings can easily be altered with the help of various parameters for example current density, duty cycle, deposition duration or time, pH of the electrolytic solution, etc. By changing time period at which the pulses are imposed, duty cycle of the coating can be varied which will change duty cycle of the coating phenomenon. The relation between the time intervals and duty cycle is given as

$$\boldsymbol{\gamma} = \frac{\boldsymbol{T_{ON}}}{\boldsymbol{T_{ON}} + \boldsymbol{T_{OFF}}}$$

Where $\boldsymbol{\gamma}$ is the duty cycle, T_{ON} is the time where the pulses are imposed and T_{OFF} is the relaxation time. Yang et al. [22] observed that with the surge in duty cycle the grain structure became coarser along with which the decrease in hardness and decrease in particle incorporation was observed. Similar observations were recorded by Lajevardi et al. [23] during the coating of Ni-TiO_2. A decrease in microhardness and TiO_2 deposition was observed with increase in duty cycles. However, researchers have only focussed on the effects of electrodeposition factors on the morphology, microstructure, hardness, corrosion and anti-wear properties and not much focus was provided for surface roughness properties.

The roughness parameters of a surface can be calculated by two methods: two dimensional (2D) or three dimensional (3D). The majority of engineering and scientific investigations have used 2D roughness analysis. Three-dimensional surface roughness, however, has become more important recently [24,25]. 2D parameters include Ra, Rq, Rt,

Rpm, Rvm, and Rz. Ra represents arithmetic average height or centre line average is the frequently used roughness parameter for quality purposes. It represents average absolute deviation from profile mean height. However, Ra cannot be deemed for the roughness, as it shows only the average of peaks and valleys. Rq is root mean square deviation from profile mean line, which is more sensitive than Ra. Rq can be more precise than Ra within the context of roughness of surfaces. The interdistance of highest peak and lowest valley over the sampling line is denoted by Rt. Rpm and Rvm embodies mean of maximum peaks and valleys in sampling length. Rz is a ten-point average or in other words it is calculated by averaging 5 x highest peaks and 5 x lowest valleys over sampling distance. Peaks are a subset of summits, which are places that are higher than their eight closest neighbours. A peak height must be greater than 5% of the surface's ten-point height in order for it to be considered a summit. All these parameters represent over the 2D plane. 3D roughness parameters include Sa, Sq, St, Spm, Svm, and Sz, which represents roughness parameters over the 3D surface. The terms are synonymous with that of 2D roughness parameters. Development of Ni-Al_2O_3 nanocoatings have been achieved in this study by varying duty cycle parameters between 20% to 100%. A modified Watts bath has been employed to contain pulse electrodeposition coating electrolyte. The microstructural properties of coated surface was evaluated using an SEM and EDS for the elemental analysis. Several studies have been conducted to assess both tribological and mechanical properties of Ni-Al_2O_3 pulse electrodeposition coating, a comprehensive study over the roughness parameters have yet to be conducted. In this work, an extensive analysis of the surface roughness properties was done for coating surface at various duty cycles from 20% to 100%. The nano hardness of the coated surface was studied with the help of a nano indenter.

2. Materials and Methods

This study presents as to how pulse electrodeposition has been employed as a coating technique. EN1A steel was employed as cathode while pure Nickel has been employed as anode. Considering the adhesive properties, availability, and cost, EN1A was made as the substrate. The cathode has been produced circular shape having 30 mm diameter and 3.5 mm height or thickness, as in disc shaped. Nickel, the anode, was rectangular with a thickness of 2 mm. The samples were polished with grit papers 220, 600, 800, and 1200 and roughness was made below 0.05 μm. After that, samples were conditioned by using acetone contained in an ultrasonic agitator for five minutes to get rid of any surface contaminants.

Table 1. Electrolytic Composition

Chemical composition	Quantity (g/L)	Function
Nickel Sulphate Hexahydrate ($NiSO_4.6H_2O$)	265	Nickel Source
Nickel (II) Chloride ($NiCl_2.6H_2O$)	48	Conductivity and Nickel Source
Boric Acid (H_3BO_3)	31	Buffering agent and Stabilizer
Aluminium Oxide (Al_2O_3)	10	Reinforcing agent

Table 2. Test conditions for coatings

	Parameter 1	Parameter 2	Parameter 3	Parameter 4	Parameter 5
Current Density (A/dm²)			3		
Duty Cycle (%)	20	40	60	80	100
Frequency (kHz)			10		
Time (min)			60		
pH			4.2 ± 0.2		
Temperature (°C)			60 ± 5		
Anode			Nickel Plate		
Cathode			EN1A		

A modified Watts Solution was used as electrolytic bath. The electrolytic chemical composition of the modified Watt Solution with their properties is shown in Table 1. Al_2O_3 with a particle size less than 50 nm (Sigma-Aldrich, Gillingham, UK) was the reinforcing material used. The constituents were magnetically stirred for 24 hours and an additional ultrasonic agitation at a frequency of 10 kHz was provided for 4 hrs. Appropriate blending and dispersion of nanoparticles in their respective electrolytes were established by magnetic agitation and ultrasonic stirring. The electrolytic solution is heated to 60 °C in final phase.

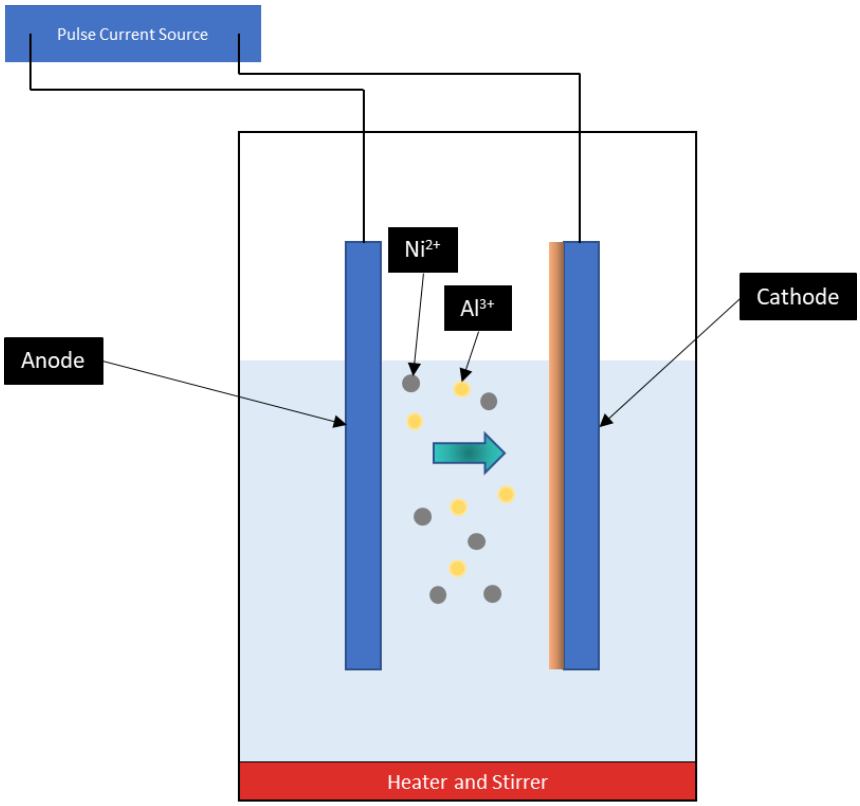

Figure 1. Schematic Diagram of Pulse electrodeposition coating

A pulse power generator was used for pulse electrodeposition coating technique. For the pulse electrodeposition coating, duty cycle was the only varying factor. All other parameters, current density, frequency, pH of electrolyte, stir speed and electrolyte temperature were kept constant. The range of the duty cycle and various other parameters were established from previous research and trials [26–31]. An increase of duty cycle from 20% to 100% has been achieved incrementally by 20%. Frequency was fixed at 10 kHz and pH was maintained at 4.2±0.2 and 3 A/dm^2 constant current density. The pulse electrodeposition was conducted at solution temperature of 60°C along with continuous magnetic stirring and ultrasonic agitation throughout the process. The coating process was set to 1 hour. After coating, distilled water was used to condition samples followed by acetone conditioning in an ultrasonic bath to remove all chemicals attached to surface. Each coating was performed 3 times to check its repeatability of the coating.

The samples were studied under a non-contact 3D optical profilometer and various parameters including Ra, Rq, Rt, Sa, Sq, St, Kurtosis, and Skewness were analysed along with power spectral density (PSD) and bearing area curve (BAC). Nanohardness of surfaces have been obtained by utilising nano indenter. Berkovich, 3-faced pyramidal, indenter was used for the study. A total of 15 indentations have been conducted on the coatings and results were analysed.

The microstructure of coating was obtained with the help of a Scanning Electron Microscope (JEOL). The grain size of coated materials was obtained with ImageJ, an open license software.

3. Results and Discussions

3.1. Surface Morphology

Fig. 2 is showing surface morphology of samples at various duty cycles. An increase in grain-size is seen with a rise in duty cycles. The electrodeposition coating with a duty cycle 20% exhibited smoothest surface. As duty cycle increases, size of particles increased. The change in grain size can be confirmed by the free energy of nucleation for new grains [32]. During T_{ON} of pulse electrodeposition coating, the nanoparticles present in the electrolyte solution will be pulled towards the cathode surface and will be embedded in them. During T_{OFF}, while current supply is cut out, loosely embedded and agglomerated particles will be detached from cathode surface and will return to electrolytic solution. This process will be repeated henceforth. With decrease in duty cycle, T_{OFF} time will be increased, as a result of which agglomeration of the particles will decrease, and grains will become finer. Once duty cycle is increased (decrease in T_{OFF} and increase in T_{ON}) particle embedding will increase resulting in more agglomerated particles. This results in decrease of nucleation rate and causes increase in grain growth [33].

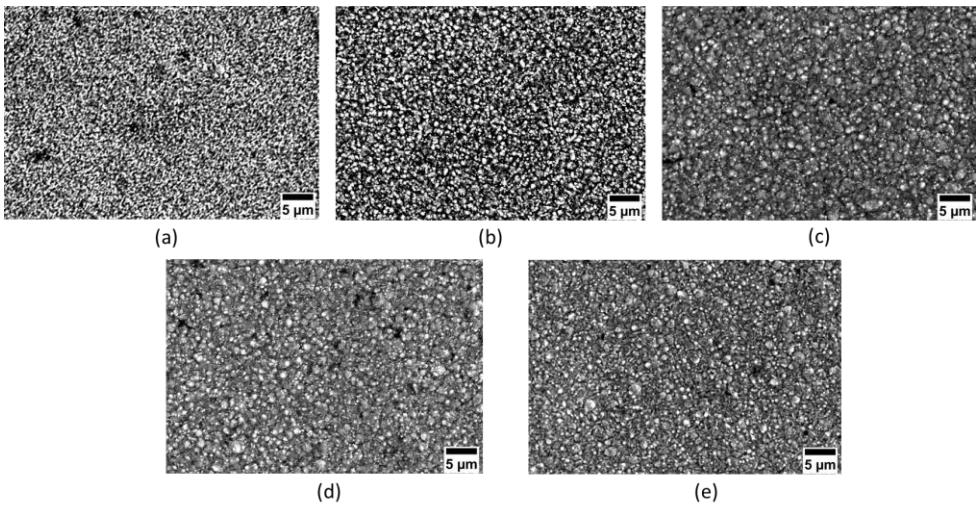

Figure 2. Scanning Electron Microscope images of coated samples at varying duty cycles (a) 20% (b) 40% (c) 60% (d) 80% and (e) 100%.

3.2. Roughness Analysis

Fig 3 show profilometer images of samples at various duty cycles. Areal roughness parameters and surface roughness parameters of all samples were analysed. Various Areal roughness parameters including Ra, Rq, Rz, Rpm, Rvm, Rt and Rz of samples at varying duty cycle is shown in Table 3. At a duty cycle of 20% Ra value was observed as 0.195 µm. Ra increased with an increase of duty cycle. Ra values were observed as 0.175 µm, 0.214 µm, 0.234 µm and 0.348 µm when duty cycles were 40%, 60%, 80% and 100% respectively. For getting more accurate Areal roughness parameters, Rq was analysed. Rq values also increased when the duty cycle has increased from 20%, 40%, 60%, 80% to 100% as 0.271 µm, 0.253 µm, 0.299 µm, 0.326 µm, 0.541 µm respectively.

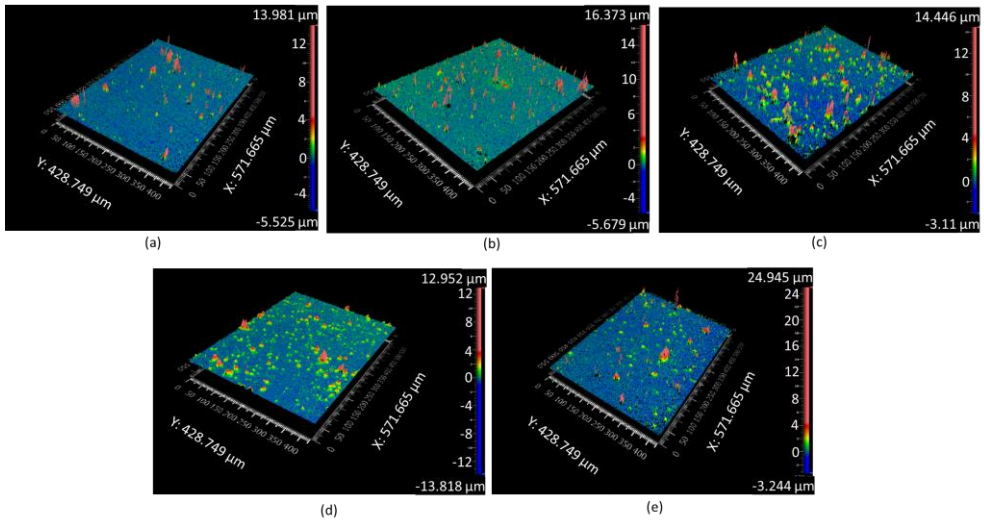

Figure 3. Profilometer images of duty cycle (a) 20%, (b) 40%, (c) 60%, (d) 80% and (e) 100%

Table 3. Areal Roughness of samples with different duty cycles

Areal Roughness paramters (µm)						
Duty Cycle	**Ra**	**Rq**	**Rpm**	**Rvm**	**Rtm**	**Rz**
20	0.195	0.271	0.781	1.043	2.125	0.752
40	0.175	0.253	0.972	1.084	1.495	0.967
60	0.214	0.299	1.244	1.155	2.549	1.998
80	0.234	0.326	1.267	1.368	2.635	2.107
100	0.348	0.541	2.748	1.550	4.299	2.857

Table 4. Surface Roughness of samples with different duty cycles

Surface Roughness (µm)						
Duty Cycle	**Sa**	**Sq**	**Spm**	**Svm**	**Stm**	**Sz**
20	0.245	0.529	14.161	7.830	19.560	15.612
40	0.277	0.682	15.865	5.345	22.212	15.974
60	0.334	0.728	16.427	3.631	22.559	16.436
80	0.371	0.742	18.948	3.531	27.479	16.687
100	0.779	1.714	23.046	4.350	27.396	16.339

The average peaks and valleys of Areal surface were also analysed. The average Areal peak height of samples increases when duty cycle increased. The 100% duty cycle samples were having the highest peak of 2.748 µm and decreased when duty cycle decreased. The peak height of 80%, 60%, 40%, and 20% was 1.267 µm, 1.244 µm, 0.972 µm, and 0.781 µm respectively. Similarly, Areal valley height of samples was analysed. The valley height increased from -1.043 µm to -1.084 µm from duty cycle 20% to 40%. Thereafter a slight decrease in height was observed as -1.155 µm at 60% duty cycle which further increased to -1.368 µm and -1.550 µm at 80% and 100% respectively. The Rt has been observed to increase when duty cycle increased from 2.125 µm to 4.299 µm at 20% and 100% duty cycles respectively.

The Rz values were analysed for obtaining a comprehensive knowledge of the average ten-point height of the profile in the sampling length. At 20% duty cycle, the Rz was observed as 0.752 µm, which increased to 0.967 µm, 1.998 µm, 2.107 µm, and 2.857 µm for

duty cycles 40%, 60%, 80%, and 100%. Therefore, it is reasonable to conclude that, with an increase in duty cycle, average maximum height difference of surface increases.

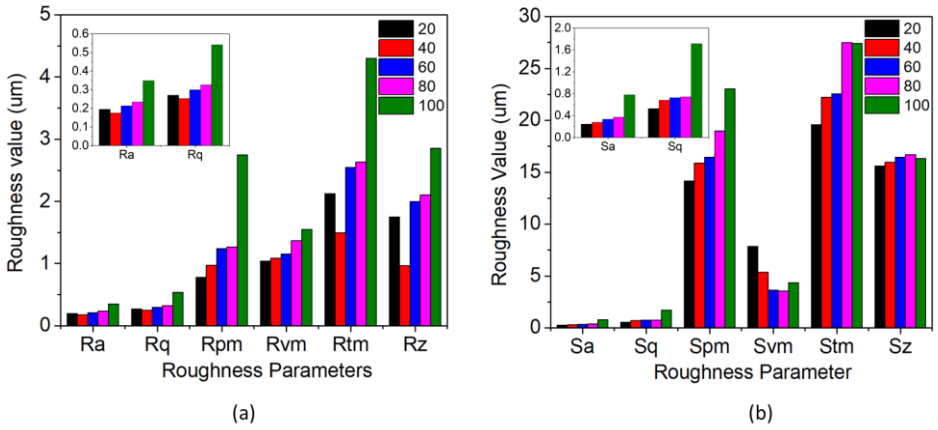

Figure 4. Areal and Surface Roughness parameters for different Duty Cycles

Surface roughness parameters have been analysed to understand roughness characteristics in the entire surface and are shown in Table 4. The surface roughness parameter calculates roughness of the whole surface whereas Areal roughness parameter will calculate roughness of the singular plane. Sa value of 20% was 0.245 μm. The Sa values increased correspondingly with duty cycle. For 40%, 60%, 80% and 100% the values were 0.277 μm, 0.334 μm, 0.371 μm, and 0.779 μm respectively. A similar increase was observed for the Sq values of 0.529 μm, 0.682 μm, 0.728 μm, 0.742 μm, and 1.714 μm for DC from 20% to 100% respectively. The average peak and average valley heights were also noted and were having a similar trend as that of the Areal roughness parameters with height increasing when duty cycle increased. Similarly for St and Sz a trend matching to that of aerial roughness properties were observed. The maximum peak height will influence the tribological properties of the surface as the peaks will restrict the complete contact of the counter surface to the material [34]. Similarly, the increase in valley height will help in the increased retention of lubricant, which will help in an improved tribological properties of the surface [34].

Table 5. Skewness and Kurtosis for various duty cycles

Skewness and Kurtosis		
Duty Cycle	**Ssk**	**Sku**
20	8.404	124.368
40	8.566	118.789
60	7.171	82.631
80	7.365	51.362
100	5.698	46.365

The variation of skewness and kurtosis with change in duty cycle was also analysed and shown in Table 5. The skewness parameter reacts strongly to isolated deep dips or extreme peaks. In the present pulse electrodeposition coating all the Ssk values are positive which implies that the surface is skewed downward relative to the mean line. The lower duty cycle samples, 20%, tends to have more peaks and filled valleys. With the rise in duty cycle from 20% to 100%, skewness decreases, which implies that the number of peaks in the surface decreases.

The measure of sharpness of peaks on a surface can be defined as kurtosis or Sku. The sharper peaks and heavier tails project positive kurtosis. The same positive kurtosis can be observed in all duty cycle samples, pointing towards the relatively high peaks and broader valleys at the surface. It can also be observed that with decline in duty cycle an growth in kurtosis value is observed. The positive excess kurtosis value projects distribution of more peaks and fatter valleys. That is, the distribution is having peaks close to the mean value and valleys which are extremely frequent than the normal distributions. These distributions are also known as leptokurtic or leptokurtotic, which will help in improving the tribological properties, by helping the lubricant to retain more on the surface [35]. The positive value of skewness and kurtosis values greater than 3, provides the insight that samples can have better tribological properties. To substantiate these findings, bearing area curves were explored and analysed. However, hardness of coating plays a similar role in tribology and has to be analysed.

3.3. Bearing area Curve

A broad-spectrum view of roughness variation can be obtained with the help of the bearing area curves which is provided in Fig 5. The variations peak-valley and the basic roughness of samples with different duty cycles can be analysed with the help of the Bearing Area Curve (BAC). Percentages of peaks, MR1 and percentages of valleys, MR2 can be obtained from the BAC. Furthermore, reduced valley-height, Svk, reduced-peak height, Spk, and core or basic roughness, Sk can be acquired from the BAC.

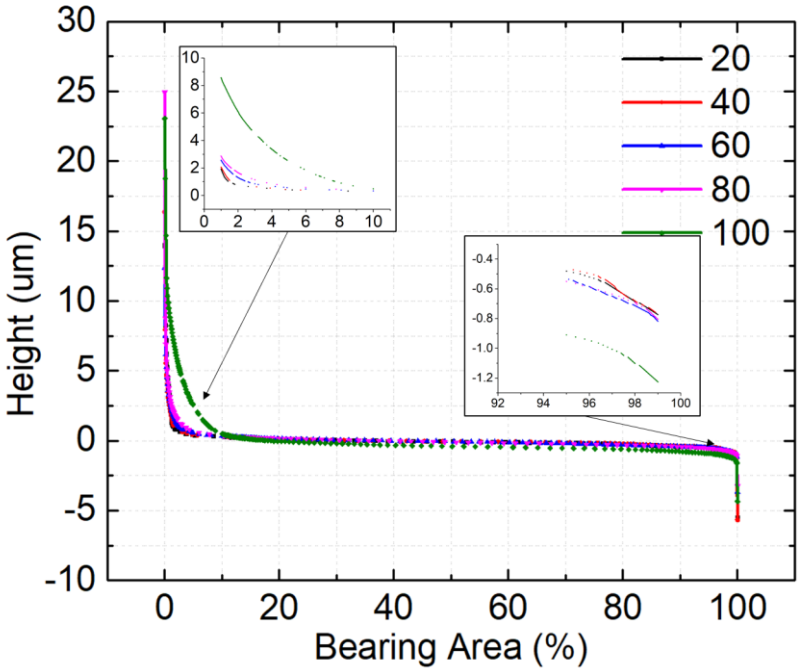

Figure 5. Bearing area curves for different Duty Cycles

From Fig 5, it can be seen that number of peaks were maximum for samples with a 100% duty cycle. When an increase in the duty cycle takes place it scores reduced number of peaks. The increased Rpk values imply that the surface is composed of a higher number of peaks. The high peaks provide a lower contact area during the tribo testing, which will result in increased contact stress. Lower surface contact area contributes to a reduction in friction and wear properties during the running in stage of tribo testing. On the other hand, the decrease in the Svk values represents the increased number of valleys in the surface below the core surface Sk. With increasing amount of valley, the lubrication

retention capacity will increase. The increase in the lubrication retention capacity will help reduce inter surfaces wear and friction values. Ratios of Spk/Sk and Svk/Sk is analysed to simplify the process. The Spk/Sk and Svk/Sk analysis will help to acknowledge whether the surface is dominated by peaks or valleys and the values are shown in Table 6. The Spk/Sk values dominate the Svk/Sk for all duty cycles. The Spk/Sk values are seen to increase with increasing duty cycle; 20% having a value of 2.03. The value increases when the duty cycle increases as 40%, 60%, 80% and 100% having a ratio of 2.77, 2.38, 2.24, 5.79 respectively. Increased number of peaks help reduce the contact area which contributes to enhancing tribological properties of interfaces. Similarly, the Svk/Sk values decreases when duty cycle increased. The values were 0.89 for 20% duty cycle which decreases to 0.54 for a duty cycle of 100% [34].

Table 6. Bearing area parameters for different duty cycles

Bearing Area Parameters									
Duty Cycle	**Rk (nm)**	**Rpk (nm)**	**Rvk (nm)**	**Rpk/Rk**	**Rvk/Rk**	**Mr1 (%)**	**Mr2 (%)**	**V1 (x 10^{13} nm^3)**	**V2 (x 10^{13} nm^3)**
20	422.495	858.300	376.515	2.032	0.891	16.74	82.885	1.920	0.769
40	423.675	1174.255	380.045	2.772	0.897	17.97	82.910	2.525	0.7865
60	567.250	1348.270	314.545	2.377	0.555	18.49	84.415	2.820	0.576
80	685.720	1535.510	364.475	2.239	0.532	19.215	90.980	3.185	0.393
100	697.960	4040.490	376.69	5.789	0.540	19.73	92.080	9.670	0.545

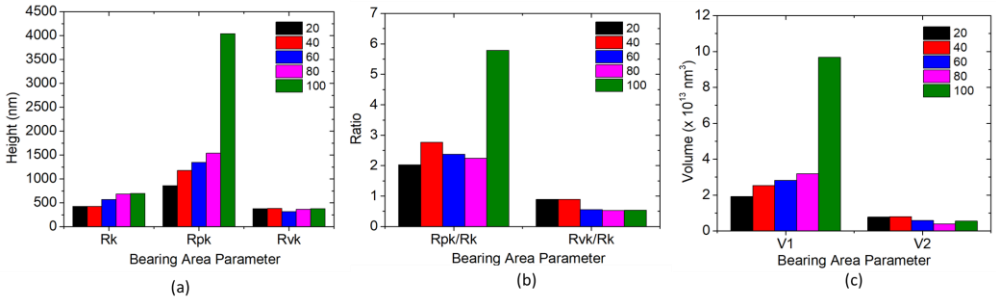

Figure 6. Bearing area parameters for different Duty Cycles

The V1 and V2 represent the material deposition profile peak area and lubricants filled profile valley area, respectively. The V1 value for 20% duty cycle was 1.92 x 10^{13} nm^3, which increased to 2.52 x 10^{13} nm^3 for duty cycle 40%. A steep increase in the V1 value was observed at 100%, 9.67 x 10^{13} nm^3. It can be concluded that the amount of the peak volume increased duty cycle increased. Whereas least amount of peak was observed at a lower duty cycle. Similar observations were seen in V2 as well. Decrease in V2 is seen when duty cycle increased. The V2 was 0.76 x 10^{13} nm^3 for 20% duty cycle which increased to 0.79 x 10^{13} nm^3 at 40% duty cycle. A decrease in value was observed at 60% and 80% duty cycle as 0.57 x 10^{13} nm^3 and 0.39 x 10^{13} nm^3 which finally increased to 0.54 x 10^{13} nm^3 for 100% duty cycle. In lieu of the surface roughness parameters, hardness values are also expected to be higher for the lower duty cycle samples.

3.4. Power Spectral Density

Fig 7 illustrates the plots exhibiting the disparity of Power Spectral Density (PSD) with spatial frequency for duty cycles 20%, 40%, 60%, 80% and 100% for x-axis and y-axis. Spatially dependent surface profiles of samples with various duty cycles, 20%, 40%, 60%, 80% and 100% were analysed in the present PSD analysis. A Fourier series decomposes input surface profile's roughness frequency (spatial frequency). Each roughness frequency's power spectral densities are recorded and averaged for PSD function calculation. Fig 7 shows results of these analyses with spatial frequency on x-axis and average roughness the RMS values on y-axis. It is evident from Fig 7 a and b that power density is high

for duty cycle 100% at lower frequency range, 0-25 /mm. For the same range, 0-25 /mm density decreases with decrease in duty cycle, with 20% having least roughness profile variation. In both cases, amplitude is seen to decrease with increase in spatial frequency. This espies that the dominating surface roughness is from mid-range and lower spatial frequencies. The power spectrum is nearly smooth in all the duty cycles after a spatial frequency of 60 /mm. the roughness frequency is independent of the flat portions with the same average roughness values [36].

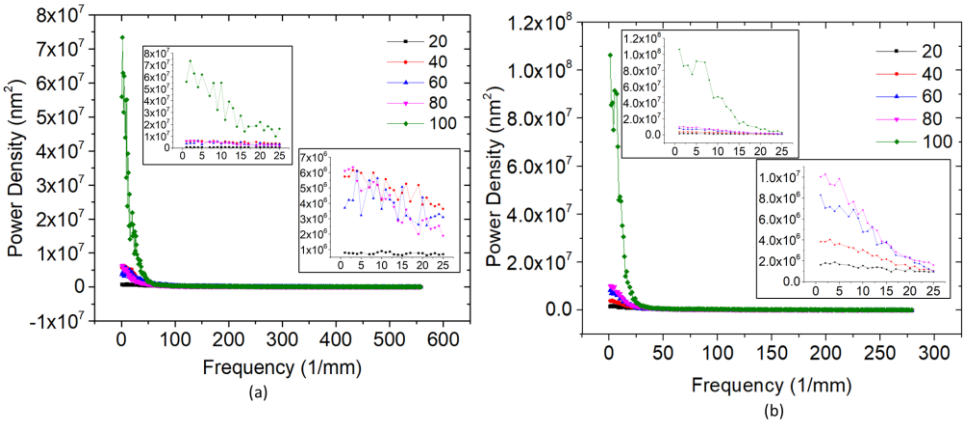

Figure 7. Power Spectral analysis for different Duty Cycles samples in (a) X-axis and (b) Y-Axis

3.5. Nanohardness

Fig 8 shows hardness pattern influenced by changes in duty cycle. It shows that the nano hardness reduced with increase in duty cycle. A significant impact was observed in nano hardness with change in the duty cycle. Maximum nano hardness was observed at a duty cycle of 20% with 4.21 GPa. For duty cycles, 40%, 60%, 80% and 100% the nano hardness was observed as 3.90 GPa, 3.86 GPa, 3.19 GPa and 3.07 GPa respectively. Results indicate that duty cycle has an impact on hardness of coating.

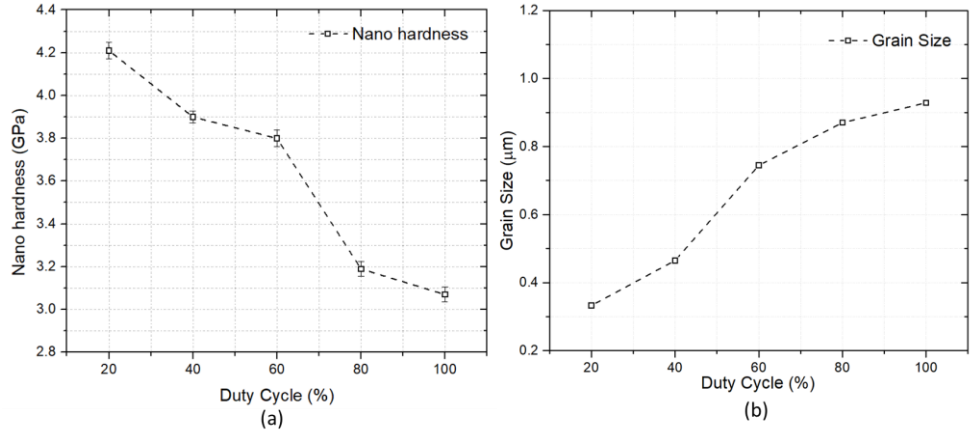

Figure 8. (a) Nanoindentation hardness for Ni-Al_2O_3 coating at different duty cycles (b) Grain size of coatings at various duty cycles

The change in hardness can be explained by the Hall-Patch equation, relating hardness and grain size.

$$HV = HV_0 + \frac{K}{\sqrt{d}}$$

Where hardness is denoted by HV, whereas HV_o and K are both constants, and d represents grain size. Coatings hardness is affected by the grains size. The increase in grain size with increasing duty cycle has already been observed earlier (Fig 2) and the grain size is calculated using an open software ImageJ. The variation of grain size with change in duty cycle is plotted in Fig 8 (b). The decrease in hardness with increase in duty cycle can be attributed to Hall Patch relationship. The higher value of nano hardness was observed for duty cycle 20% which will provide a better wear properties.

4. Conclusions

In this study electrodeposition with varying duty cycles from 20% to 100% has been employed for developing Ni-Al_2O_3 nanocomposite. Various Areal and surface roughness properties of nanocomposite coatings have been analysed. It was observed that the roughness values increased when duty cycle increased. Both the skewness and kurtosis values of surfaces were analysed and were observed that skewness decreased with increased duty cycle. Similarly, with an increase in duty cycle, kurtosis was also seen to decrease. However, all duty cycle were having kurtosis greater than 3 and positive skewness. Positive skewness and higher kurtosis will help in reduction of friction, which points that 20% duty cycle has the best wear properties. The nano hardness of samples was analysed and was observed that lower duty cycle was having higher hardness, which helps to improve tribological properties of surface. Decrease in nano hardness at higher duty cycle was due to increase in grain size resulting from shorter OFF time.

Author Contributions: For research articles with several authors, a short paragraph specifying their individual contributions must be provided. The following statements should be used "Conceptualization, AJ ; methodology, AJ and ZK; software, AJ; validation, AJ; formal analysis, AJ; investigation, ZK; resources, AJ; data curation, AJ; writing—original draft preparation, AJ, AS and ZK; writing—review and editing, AJ; visualization, AS and ZK; supervision, ZK; project administration, ZK; funding acquisition, All authors have read and agreed to the published version of the manuscript.

Funding: No funding has been received to conduct this research.

Informed Consent Statement: The authors declare no conflict of interest.

Acknowledgments: The authors would like to acknowledge Mr George Foot ASMPT SMT UK Ltd for their in-kind support.

Conflicts of Interest: The authors declare no conflict of interest

References

1. Xue, Z.; Lei, W.; Wang, Y.; Qian, H.; Li, Q. Effect of pulse duty cycle on mechanical properties and microstructure of nickel-graphene composite coating produced by pulse electrodeposition under supercritical carbon dioxide. *Surf Coat Technol* **2017**, *325*, 417–428.

2. Wang, W.; Hou, F. Y.; Wang, H.; Guo, H. T. Fabrication and characterization of Ni-ZrO2 composite nano-coatings by pulse electrodeposition. *Scr Mater* **2005**, *53*, 613–618.

3. Zhang, Y.; Zhang, S.; He, Y.; Li, H.; He, T.; Fan, Y.; Zhang, H. Mechanical properties and corrosion resistance of pulse electrodeposited Ni-B/B4C composite coatings. *Surf Coat Technol* **2021**, *421*.

4. Vamsi, M. V. N.; Wasekar, N. P.; Sundararajan, G. Influence of heat treatment on microstructure and mechanical properties of pulse electrodeposited Ni-W alloy coatings. *Surf Coat Technol* **2017**, *319*, 403–414.

5. Wasekar, N. P.; Latha, S. M.; Ramakrishna, M.; Rao, D. S.; Sundararajan, G. Pulsed electrodeposition and mechanical properties of Ni-W/SiC nano-composite coatings. *Mater Des* **2016**, *112*, 140–150.

6. Li, Q.; Yang, X.; Zhang, L.; Wang, J.; Chen, B. Corrosion resistance and mechanical properties of pulse electrodeposited Ni-TiO2 composite coating for sintered NdFeB magnet. *J Alloys Compd* **2009**, *482*, 339–344.

7. Bahadormanesh, B.; Dolati, A. The kinetics of Ni-Co/SiC composite coatings electrodeposition. *J Alloys Compd* **2010**, *504*, 514–518.
8. Alizadeh, M.; Mirak, M.; Salahinejad, E.; Ghaffari, M.; Amini, R.; Roosta, A. Structural characterization of electro-codeposited Ni-Al2O 3-SiC nanocomposite coatings. *J Alloys Compd* **2014**, *611*, 161–166.
9. Allahkaram, S. R.; Golroh, S.; Mohammadalipour, M. Properties of Al2O3 nano-particle reinforced copper matrix composite coatings prepared by pulse and direct current electroplating. *Mater Des* **2011**, *32*, 4478–4484.
10. Lodhi, Z. F.; Mol, J. M. C.; Hovestad, A.; Terryn, H.; de Wit, J. H. W. Electrodeposition of Zn-Co and Zn-Co-Fe alloys from acidic chloride electrolytes. *Surf Coat Technol* **2007**, *202*, 84–90.
11. Li, H.; He, Y.; Luo, P.; Fan, Y.; Yu, H.; Wang, Y.; He, T.; Li, Z.; Zhang, H. Influence of pulse frequency on corrosion resistance and mechanical properties of Ni-W/B4C composite coatings. *Colloids Surf A Physicochem Eng Asp* **2021**, *629*.
12. Wasekar, N. P.; Sundararajan, G. Sliding wear behavior of electrodeposited Ni-W alloy and hard chrome coatings. *Wear* **2015**, *342–343*, 340–348.
13. Jiang, W.; Shen, L.; Xu, M.; Wang, Z.; Tian, Z. Mechanical properties and corrosion resistance of Ni-Co-SiC composite coatings by magnetic field-induced jet electrodeposition. *J Alloys Compd* **2019**, *791*, 847–855.
14. Imaz, N.; García-Lecina, E.; Suárez, C.; Díez, J. A.; Rodríguez, J.; Molina, J.; García-Navas, V. Influence of additives and plating parameters on morphology and mechanical properties of copper coatings obtained by pulse electrodeposition. *Transactions of the Institute of Metal Finishing* **2009**, *87*, 64–71.
15. Lausmannl, G. A. *Electrolytically deposited hardchrome*; 1996; Vol. 86.
16. Bahrololoom, M. E.; Sani, R. The influence of pulse plating parameters on the hardness and wear resistance of nickel-alumina composite coatings. *Surf Coat Technol* **2005**, *192*, 154–163.
17. Jegan, A.; Venkatesan, R. Characterization and optimization of pulse electrodeposition of Ni/nano-Al2O3 composite coatings. *International Journal of Minerals, Metallurgy and Materials* **2013**, *20*, 479–485.
18. Chen, L.; Wang, L.; Zeng, Z.; Xu, T. Influence of pulse frequency on the microstructure and wear resistance of electrodeposited Ni-Al2O3 composite coatings. *Surf Coat Technol* **2006**, *201*, 599–605.
19. Steinbach, J.; Ferkel, H. Nanostructured Ni-Al2O3 films prepared by DC and pulsed DC electroplating. *Scr Mater* **2001**, *44*, 1813–1816.
20. Ma, C. Y.; Zhao, D. Q.; Xia, F. F.; Xia, H.; Williams, T.; Xing, H. Y. Ultrasonic-assisted electrodeposition of Ni-Al2O3 nanocomposites at various ultrasonic powers. *Ceram Int* **2020**, *46*, 6115–6123.
21. Gül, H.; Uysal, M.; Akbulut, H.; Alp, A. Effect of PC electrodeposition on the structure and tribological behavior of Ni-Al2O3 nanocomposite coatings. *Surf Coat Technol* **2014**, *258*, 1202–1211.
22. Yang, Y.; Cheng, Y. F. Fabrication of Ni-Co-SiC composite coatings by pulse electrodeposition - Effects of duty cycle and pulse frequency. *Surf Coat Technol* **2013**, *216*, 282–288.
23. Lajevardi, S. A.; Shahrabi, T. Effects of pulse electrodeposition parameters on the properties of Ni-TiO 2 nanocomposite coatings. *Appl Surf Sci* **2010**, *256*, 6775–6781.
24. Jackson, R. L. Lubrication. *Handbook of Lubrication and Tribology, Volume II: Theory and Design, Second Edition* **2012**, *123*, 14-1-14–14.
25. Sedlaček, M.; Podgornik, B.; Vižintin, J. Influence of surface preparation on roughness parameters, friction and wear. *Wear* **2009**, *266*, 482–487.
26. Bajwa, R.; Khan, Z.; Nazir, H.; Chacko, V.; Saeed, A. Wear and friction properties of electrodeposited Ni-based coatings subject to nano-enhanced lubricant and composite coating. *Acta Metallurgica Sinica (English Letters)* **2016**, *29*, 902–910.

27. Bhutta, M. U.; Khan, Z. A.; Garland, N. Wear performance analysis of Ni-Al 2 O 3 nanocomposite coatings under nonconventional lubrication. *Materials* **2018**, *12*.
28. Bhutta, M. U.; Khan, Z. A. Wear and friction performance evaluation of nickel based nanocomposite coatings under refrigerant lubrication. *Tribol Int* **2020**, *148*, 106312.
29. Nazir, M. H.; Khan, Z. A.; Saeed, A.; Bakolas, V.; Braun, W.; Bajwa, R.; Rafique, S. Analyzing and modelling the corrosion behavior of Ni/Al2O3, Ni/SiC, Ni/ZrO2 and Ni/graphene nanocomposite coatings. *Materials* **2017**, *10*.
30. Bajwa, R. S.; Khan, Z.; Bakolas, V.; Braun, W. Effect of bath ionic strength on adhesion and tribological properties of pure nickel and Ni-based nanocomposite coatings. *J Adhes Sci Technol* **2016**, *30*, 653–665.
31. Bajwa, R. S.; Khan, Z.; Bakolas, V.; Braun, W. Water-lubricated Ni-based composite (Ni-Al2O3, Ni-SiC and Ni-ZrO2) thin film coatings for industrial applications. *Acta Metallurgica Sinica (English Letters)* **2016**, *29*, 8–16.
32. Yang, Y.; Cheng, Y. F. Fabrication of Ni-Co-SiC composite coatings by pulse electrodeposition - Effects of duty cycle and pulse frequency. *Surf Coat Technol* **2013**, *216*, 282–288.
33. Wang, L.; Zhang, J.; Gao, Y.; Xue, Q.; Hu, L.; Xu, T. Grain size effect in corrosion behavior of electrodeposited nanocrystalline Ni coatings in alkaline solution. *Scr Mater* **2006**, *55*, 657–660.
34. Edachery, V.; John, A.; Rajendran, A.; Srinivasappa, V.; Mathiyalagan, S.; Kumar, S.; Kailas, S. V. Enhancing tribological properties of Inconel X-750 superalloy through surface topography modification by shot blasting. *Mater Perform Charact* **2021**, *10*, 322–332.
35. Sedlaček, M.; Podgornik, B.; Vižintin, J. Correlation between standard roughness parameters skewness and kurtosis and tribological behaviour of contact surfaces. *Tribol Int* **2012**, *48*, 102–112.
36. Edachery, V.; Swamybabu, V.; Adarsh, D.; Kailas, S. v. Influence of surface roughness frequencies and roughness parameters on lubricant wettability transitions in micro-nano scale hierarchical surfaces. *Tribol Int* **2022**, *165*, 107316.